Experimental Investigation of the Effect of Surface Geometry on Spray Impingement and Its Macroscopic Behaviour

Christoph Steinberg[1], Huijia Lv[1],David L.S. Hung[*,1,2], Xuesong Li[2], Min Xu[2]
[1]University of Michigan-Shanghai Jiao Tong University Joint Institute, Shanghai Jiao Tong University, 200240 Shanghai, P.R. China
[2]Institute of Automotive Engineering, School of Mechanical Engineering, Shanghai Jiao Tong University, 200240 Shanghai, P.R. China
*Corresponding author: dhung@sjtu.edu.cn

Abstract

The injection of fuel in a combustion engine cylinder is a highly transient and very complex process which dictates the performance and emissions of engines. Increasing the injection pressure or injecting fuel during late compression stroke tend to increase the combustion efficiency and decrease emissions. However, excessive fuel impingement on piston top and cylinder walls could become major negative issues resulting in very inhomogeneous mixture formation, incomplete combustion, considerable cycle-to-cycle variation, and increased fuel film formation. It is generally assumed that the shape of the piston top has a profound impact on the behaviour on spray impingement, spray propagation, fuel vaporisation as well as the cycle-to-cycle variation. This work investigates the spray impingement on surface with various geometrical configurations to develop a deeper understanding of the macroscopic spray behaviour. High-speed mie-scattering visualisations of spray impact on surfaces in a constant volume chamber are conducted. A parametric analysis with three surface geometries of stepped configurations with slope of 30°, 60°, and 90° is carried out. Probability Presence Images are created to evaluate the cycle-to-cycle variations and their effects when the spray impinges on the surface. It reveals that the surface geometry has an immense effect on the spray propagation and, therefore, on the vaporisation process. On one hand, the geometry can stretch the spray and improve the spreading of the fuel, indicating an enhanced vaporisation. On the other hand, the geometry can also constrict the propagation and thus delay the vaporisation. Additionally, by focussing on the cycle-to-cycle variation, significant differences in the impingement process and propagation behaviour are elucidated. For instance, the spray propagation in different cycles develop different film thicknesses and vortex behaviour. Results imply that the impinging geometry could either amplify or weaken a vortex behaviour. This work should establish a link between the surface geometry and the spray behaviour both qualitatively and quantitatively. In addition, the influence of the geometry on the cycle-to-cycle variation will be investigated towards to possibility if the impinging geometry is feasible to dampen the effect of cycle-to-cycle variation while enhancing the vaporisation process.

Keywords

high-speed visualization, fuel spray impingement, cycle-to-cycle variations, surface geometry, macroscopic spray behaviour

Introduction

Nowadays, combustion engines face strong challenges related to reducing emissions and increasing combustion efficiency. Tackling these issues, fuel injector technologies are designed to increase the injection pressure; but when combining with multiple injection strategy or delaying the fuel injection to a later time at compression stroke, fuel spray impingement on cylinder walls becomes unavoidable. Hence, the evolution of an exorbitant fuel film on piston top and cylinder walls could cause major negative issues. Easing the fuel vaporisation results in a very inhomogeneous air-fuel mixture which leads to incomplete combustion with strong cycle-to-cycle variations [1] [2]. An increased fuel film formation might retain during the combustion phase which ultimately becomes a source of hydrocarbon (HC) and particulate matter (PM) [3] [4]. Recently, Schulz et al. [2] investigated the parameters on the wall film development. The fuel film mass reduces when the following parameters increase: fuel temperature, ambient temperature, injection pressure and the distance between injector tip and wall. Akop et al. [5] observed experimentally on an inclined plate that an increase in injection pressure causes a liquid film thickness to decrease. In addition, a steeper inclination of the plate decreases the adhered fuel mass ratio. Moreover, Suh et al. [6] found out that a larger inclination of the wall and higher injection pressure enlarge the radial spray tip penetration. Furthermore, a larger inclination also promotes the vortex formation. Optical measurement techniques such as high-speed mie-scattering became a popular method to investigate the behaviour of impinging sprays to determine the evolution of the spray envelope [7]. Therefore, several spray impinging studies on a flat plate revealing the effects of injection pressure, ambient pressure, wall temperature, and injection distance to the plate have been conducted [4], [8], [9], and [10]. Increasing the impinging distance causes a higher probability for the droplets to adhere instead of bouncing back from the wall, which leads to an increase in maximum film thickness and a decrease of film uniformity [11].

Furthermore, droplets with high tangential velocity might float away due to the lift force by the boundary layer and, therefore, do not impinge [12]. In addition, the wall surface roughness provokes a shorter spray tip penetration and a less uniform fuel film distribution, whereas the impinging height grows [9]. Shim et al. [13] investigated the spray development in a cavity with different wall angles experimentally and numerically. It was found that the geometry restrains the spray propagation after impinging, which depends on the wall angle and the density distribution of the spray. Subsequently, it affects the vaporisation time of the fuel as well as the vortex behaviour. Fan et al. [14] used two different piston heads for the spray-wall impingement investigation. It was shown that the propagation and behaviour of the spray is highly influenced by the surface geometry. However, not much research has been focussed on the geometry effect of an impinging spray yet.

The second focus of this research is the effect of cycle-to-cycle variations. Severe cycle-to-cycle variations of engine combustion increase the covariance of the indicated mean effective pressure in the cylinder [15] resulting in combustion instability which intensifies engine roughness and vibrations. For investigating the cycle-to-cycle variations of spray structures, the *Probability Presence Image* method has been employed by Hung et al. [16] to assess these variations quantitatively. Later, Zhong et al. [17] used this method to examine the cycle-to-cycle variations of a multi-hole solenoid-actuated fuel injector with n-hexane where strong variations at the spray tip are detected. In the current study, the *Probability Presence Image* method is applied. For the analysis, image processing is used and, therefore, it is crucial to identify the spray from the background. Specifically, it is important to set a reasonable threshold to extract the spray boundary from the background. A wide literature research of threshold techniques has been done by Sezgin et al. [18]. Mostly a fixed threshold is used when investigating fuel sprays [19] which is determined by a subjective approach. However, the threshold is sensitive towards the spray pattern determination. A small threshold cannot distinguish between spray and background, whereas a high threshold might fail to show important spray behaviour.

This work bridges the gap from existing impinging spray research to more complex spray conditions occurring in internal combustion engines since modern piston tops tend to follow complex geometries. For an inclined spray, where backward and forward movement pursue different behaviours, it investigates how a surface geometry is able to alter these distinctive behaviours. Therefore, experiments in a constant volume chamber using high-speed mie-scattering visualisation are conducted. Three surface geometries of stepped configurations with slope of 30°, 60° and 90° are examined in a preliminary parametric analysis. The data analysis is focussed on the macroscopic transient behaviour of the spray to elucidate the geometry effect by revealing the intensity distributions and cycle-to-cycle variations. Finally, the findings should be valuable for other spray impingement application such as spray cooling or painting purposes.

Methodologies and Experimental Setup

The measurements were conducted with high-speed-imaging in order to evaluate the macroscopic spray behaviour quantitatively and qualitatively (Fig. 1a). In a constant volume chamber, a polished sapphire plate of 110 mm diameter with a thickness of 3 mm was used as the flat plate. As the geometry, blocks made of fused silica with different slopes were utilized. The surface roughness R_a of the flat plate and the geometry blocks were measured to be 29.8 nm and 9.1 nm, respectively.

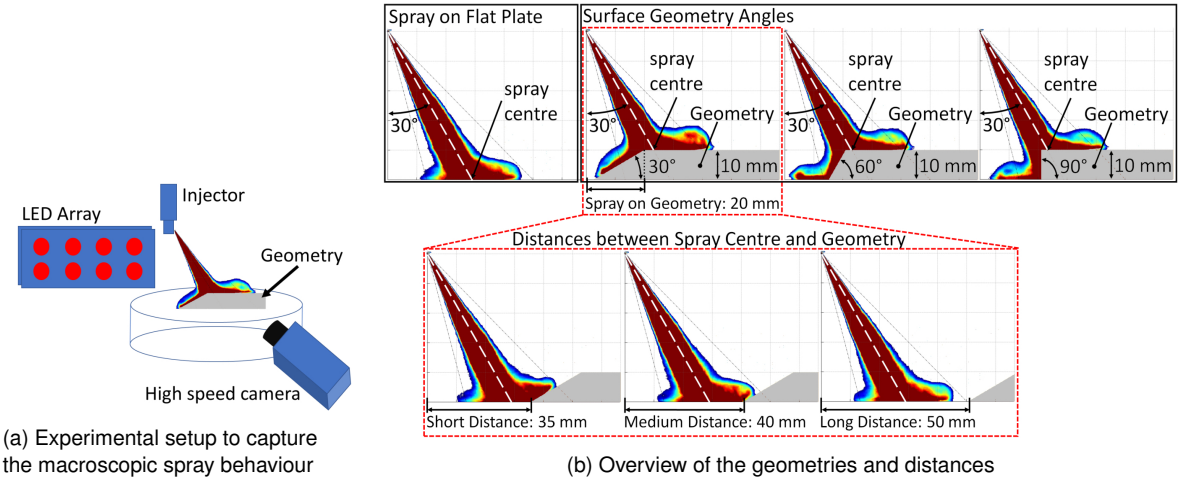

(a) Experimental setup to capture the macroscopic spray behaviour

(b) Overview of the geometries and distances

Figure 1. Measurement setup and geometries

A single-hole injector with an inner diameter of 0.2 mm, a nozzle length to diameter ratio of 1.5 and an impingement angle of *30°* was applied. N-hexane was used as the fuel which was injected at 15 MPa for a duration of

1.5 ms. The vertical distance between injector tip and impingement plate was 52 mm. The ambient pressure was 101 kPa and the temperatures of fuel and ambient air were both set at 20°.
A 2x4 red light LED array illuminated the spray droplets through mie-scattering which were captured by a high-speed, synchronised camera (Phantom V1210). The image was 12-bit grayscale with a total of 4096 levels of intensity. The test cases in this research include three geometries and a flat plate as reference. The geometries were a step with slope of 30°, 60° and 90° (Fig. 1b), each 10 mm high. Furthermore, the distance between the spray axis and the step geometry was varied from 20 mm to 50 mm. In the 20 mm case, the spray impinged directly on the step geometry, whereas in all other cases the fuel impinged on the flat plate firstly and subsequently propagated towards the step geometry. All in all, 13 cases were examined with 10 cycles for each case to assess the cycle-to-cycle variations. For the analysis, every 0.05 ms an image was extracted and processed by an in-house Matlab code.

Spray Image Analysis

The analysis of the spray impingement images is carried out considering *Wetted Lengths*, *Average Value Images*, and *Probability Presence Images*. In the Fig. 2a, the *Wetted Length* is defined as the length where the surface is in contact with the fuel. This value gives an indicator about the propagation of the fuel and helps to categorize if a geometry promotes the propagation or suppresses it. In addition, the images of 10 cycles are composed to form an *Average Value Image* showing the intensity distribution to examine the propagation behaviour. That might not reflect the detailed behaviour of a single cycle but gives an understanding of the overall characteristics of the propagation behaviour, what intensity distributions are expected, and what overlaying structures are shown. A fixed intensity value of 100 is used as the threshold because it clearly shows the boundary of the spray envelope to the background noise which has an average intensity value of around 20. Therefore, a fixed threshold value is suitable. For a better contrast to the background noise, intensity values less than 100 are not considered when creating the images with the in-house Matlab code. Due to the methodology, the vaporisation process can be estimated but only limited data is available to describe it precisely since the spray is seen from a two-dimensional plane. Also, it is not certain if the intensity reflects the density of the spray or a possible out-of-plane flow. In order to investigate the cycle-to-cycle variations quantitatively, the *Probability Presence Image* technique is applied [16] [17]. The *Probability Presence Image* evaluates the probability of the presence of fuel over all cycles. The procedure to obtain the *Probability Presence Image* is depicted in Fig. 2c. Firstly, the images are binarized according to a certain threshold intensity, then divided pixel-by-pixel by the number of cycles and summed up pixel-by-pixel over all cycles. The results are images depicting the probability of the presence of fuel. For the binarizing step, an intensity value of 250 is used to capture detailed differences between the cycles such as vortex behaviour. When choosing a too high or too less threshold, the details in the spray propagation could vanish. However, since the raw images are binarized during the process, the intensity distribution and characteristics of the spray structure are neglected and only the spray envelope is considered.

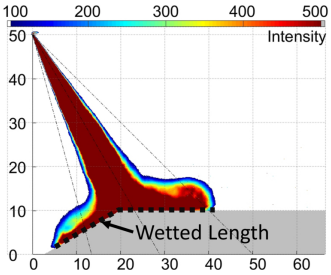

(a) Definition of *Wetted Length*

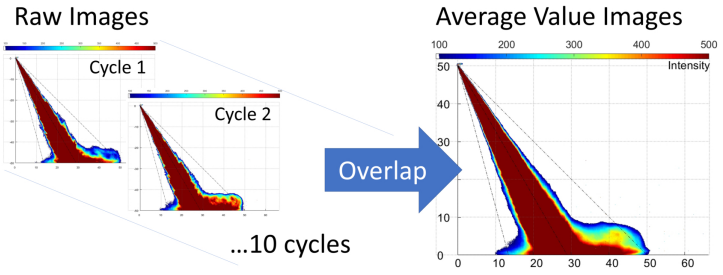

(b) Procedure of the *Average Values Images*

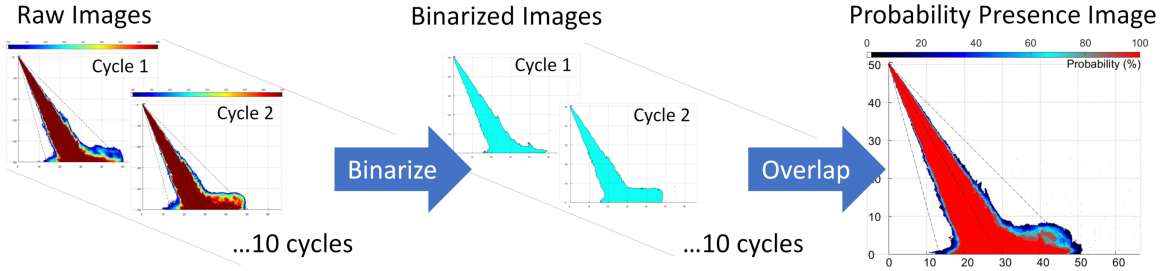

(c) Procedure of the *Probability Presence Images*

Figure 2. Methodologies for the multiple cycle analysis

Spray Characteristics before Impact and Consequences of the Impinging Process

The spray characteristics in the free spray vary due to fluctuations caused by the internal flow inside the nozzle and dissipation with the surrounding air. In cases where the spray touches the flat plate first, different behaviour of the spray tip at the touching time occurs, such as an "upside down V" (Fig. 3a) with two touching points or an "upside down L" (Fig. 3b) with only one touching point. The situation with the 20 mm cases is different (Fig. 3c). The spray pattern between the cases are far less distinctive since the shorter distance does not allow the spray to develop strong characteristics before impinging. However, the propagation in these cases is highly determined by the geometry of the impinging surface.

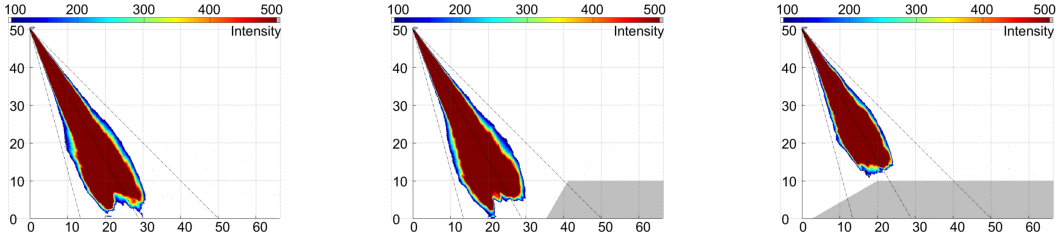

(a) Upside down "V" (b) Upside down "L" (c) No strong characteristic

Figure 3. Different spray characteristics before impinging

For comparison purposes and to demonstrate the consequence of a spray impinging on a flat plate, the spray envelopes are transferred into contour images. Figure 4 shows the spray envelope shortly before and after impinging for the flat case and cases with a long distance to the geometry. To pinpoint the consequence of the impinging process, any influence of the geometry is neglected. At time step 0.50 ms (Fig. 4a), it shows that the boundaries of the spray envelope differ strongly at the spray tip. However, when time elapses and the impinging process progresses, the differences decrease to only minimal variations (Fig. 4b). Therefore, the impinging process exhibits a "filter" effect towards spray tip variations which determines the flow movement until the geometry effect dictates further propagation. However, although the spray envelope varies slightly between the cases at 0.75 ms and at 1.00 ms, the intensity distribution starts to differ between the cases with time. At 0.75 ms, the variations in the intensity distribution are small, whereas at 1.00 ms the differences are more severe. These changes finally lead to different behaviour such as the development of a vortex on the right side.

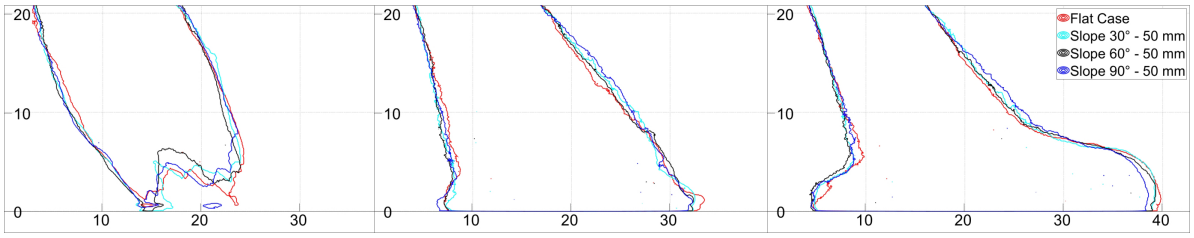

(a) Spray tip at 0.50 ms (b) Spray tip at 0.75 ms (c) Spray tip at 1.00 ms

Figure 4. Contour comparison in the 50 mm distance cases

Geometry Effect

1.) Flat case as reference

In a first step, the flat case is analysed as a reference for comparing and assessing the geometry effect on the spray propagation. After the start of the injection, the spray propagates and tears off due to friction with the surrounding air. When impinging, a spray cone develops and the propagation starts developing towards both sides (Fig. 6a-b). Soon after, the propagation to the left side slows down and shows a lower intensity (intensity value < 500) suggesting the beginning of the vaporisation process. However, the fuel spreads out to the right side accompanied with vortex behaviour and, at later stage, a decrease of intensity indicates an advanced vaporisation process.

2.) Impinging spray on geometry

Figure 5 depicts the *Wetted Length* of the geometry cases compared to the flat case. It is shown that the step geometry enlarges the spreading of the fuel (20 mm case) or highly constrains the propagation (35 mm case). Increasing the distance to the step geometry weakens the influence of the geometry on the flow.

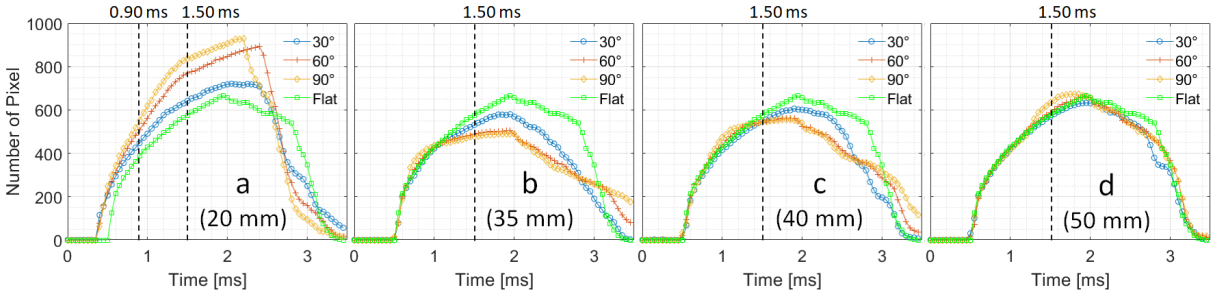

Figure 5. *Wetted Lengths* at distance 20 mm (a), 35 mm (b), 40 mm (c) and 50 mm (d)

In the 20 mm case, the spray hits the step geometry first which divides the propagation into two main directions resulting in a rise up to 30% of the *Wetted Length*. In the 30° case (Fig. 6c-d), the slope is perpendicular to the spray direction causing the spray droplets to bounce back which leads to higher resistance for the propagation on the left side. Furthermore, the higher resistance weakens the kinetic energy of the flow due to the slope angle which limits the movement significantly. Therefore, more fuel flows to the right side shown in the higher flow thickness and a vortex behaviour is more likely to occur.

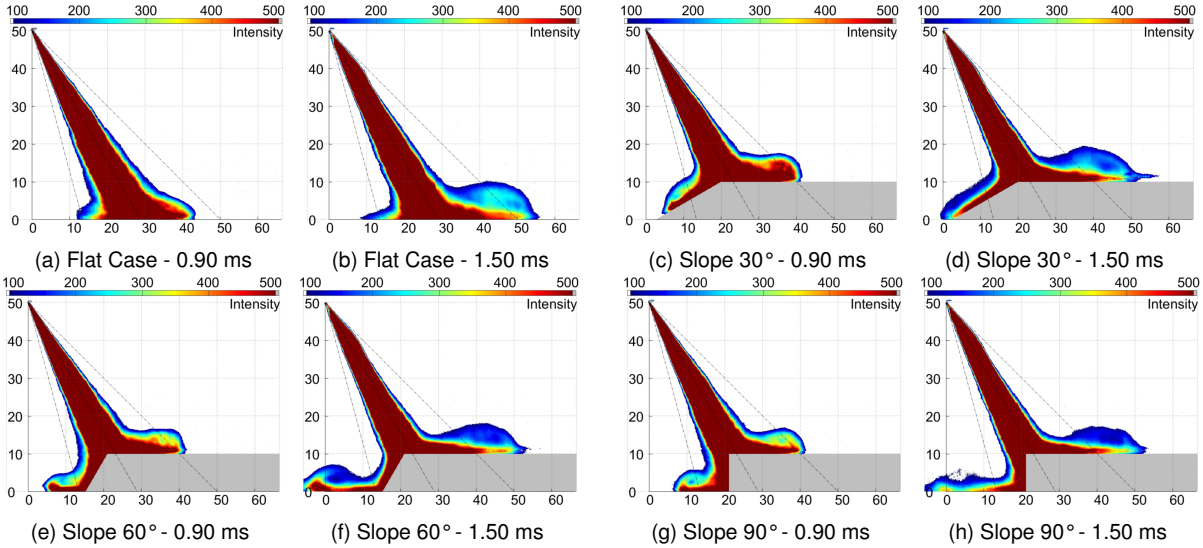

Figure 6. *Average Values Images* with 20 mm distance (scale of x- and y-axis in mm)

While increasing the step geometry angle to 60° and 90° (Fig. 6e-h), the flow resistance is gradually decreased and more liquid passes on the left side provoking a shrinkage of the film thickness on the right side. Furthermore, both step geometries boost the expansion of the fuel and provoke a vortex on the tip of the left side. Particularly in the 90° case, it is assumed that there is an increased out-of-plane propagation along the slope or step contour. In addition, the abrupt transition to the flat case might cause turbulence in the flow. After the *Wetted Length* reaches its maximum in the 60° and 90° cases, there is a drastic decrease most likely due to the large spreading which boosts the vaporisation process. However, the 30° case shows a deteriorated vaporisation process (>2.7 ms)(Fig. 5a) possibly because of the higher flow resistance and larger film thickness on the slope, and the fuel remains longer on the upper edge of the slope.

In the 35 mm case (Fig. 7a), the spray impacts on the flat plate first and then propagates towards the step. It is evident that the step geometry significantly constrains the spray propagation leading to a drastic change in the *Wetted Length* (Fig. 5b) and the loss can be up to 25% compared to the flat case. The *Wetted Length* in the 60° and 90° case only differs in the late vaporisation process (>3.0 ms). Moreover, it is shown that the shape of the geometry highly governs the direction of the propagation since the flow does not spread along the horizontal direction of the step geometry (Fig. 7). Additionally, with increasing step angle, the low intensity area decreases and the spray becomes denser. Although the right side is constrained by the step, surprisingly the propagation to the left side does not significantly enlarge. Reasons for that behaviour could be the propagation along the out-of-plane direction (especially in the 90° case) and/or an increase of the density of the spray in the constrained area. Due to the limited propagation on the right side, it is shown in Fig. 5b that the vaporisation process is strongly delayed.

Consequently, with increasing the distance to 40 mm (Fig. 7b) between step geometry and spray axis, the constraining effect becomes weaker since the spray hits the geometry at a later time. Therefore, the *Wetted Length*

decreases and the difference in the maximum propagation compared to the flat case shrinks to around 15%. Subsequently, in the 50 mm case (Fig. 7c), the spray hits the step geometry almost at the end of the injection. Therefore, the *Wetted Length* is close to the flat case but still shows a small constraining effect after the end of injection (>1.50 ms). In the 90° case, a rise between 1.25 ms and 1.75 ms is shown since the spray reaches the vertical side of the step geometry which increases the *Wetted Length* suddenly. Moreover, due to the constraint, the intensity on the right side is increased compared to the flat case (Fig. 7c). Also, it seems that the constraint supports the vortex behaviour on the right side.

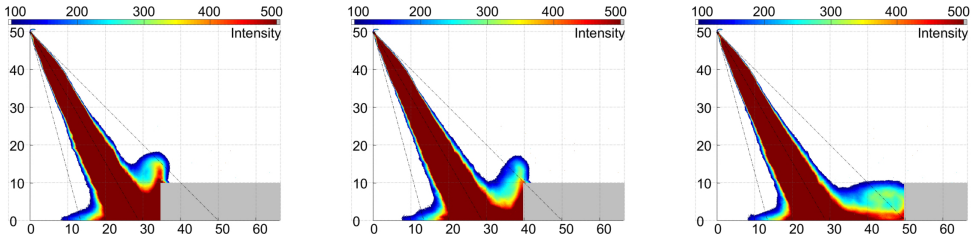

(a) 90° Slope - 35 mm (b) 90° Slope - 40 mm (c) 90° Slope - 50 mm

Figure 7. *Average Value Images* in the 90° case at time step 1.50 ms (scale of x- and y-axis in mm)

Cycle-to-Cycle Variations

In order to assess the cycle-to-cycle variations, the *Presence Probability Image* technique with a threshold intensity of 250 is used. To examine the variations, the overlap ratio percentage of the high probability (100% of the cycle) and the low probability (area which is covered by at least one cycle) is introduced

$$\textit{Overlap Area Ratio} = \frac{\textit{Area High Probability}}{\textit{Area Low Probability}} \cdot 100(\%). \tag{1}$$

1.) Flat case as reference

In the flat case, the *Overlap Area Ratio* increases after the injection while the free spray develops (Fig. 8a). Shortly before impinging (around 0.5 ms), the cycle-to-cycle variations are strongest as indicated by a low overlap area (62%) which is the lowest value until the end of injection. Afterwards, the sides of the spray cone are affected by the variations resulting in a rise of the overlap (74% at around 1.00 ms) due to the constraint of the flat plate (Fig. 9a). With increasing time, the cycle-to-cycle variations increase on the right side indicating a strong difference of the propagation of the cycles or the possibility of a vortex behaviour in some cycles (Fig. 9b).

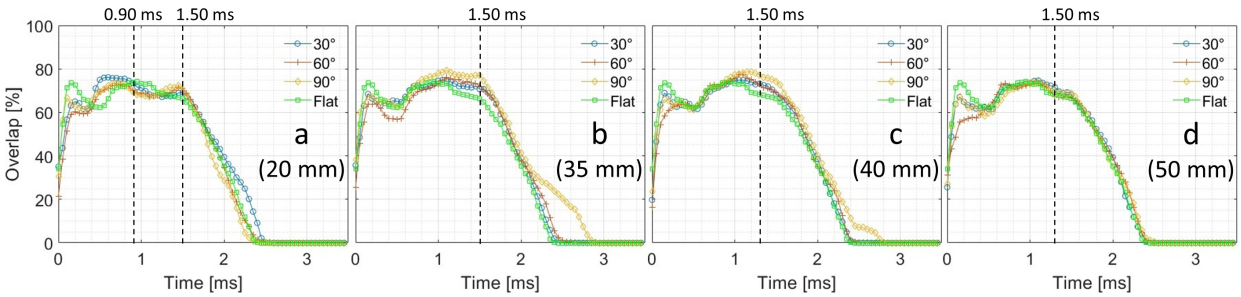

Figure 8. *Overlap Areas* with distance 20 mm (a), 35 mm (b), 40 mm (c) and 50 mm (d)

2.) Impinging spray on geometry

Figure 8 depicts the *Overlap Area Ratio* over the time and distance variation to the step geometry compared to the flat case. It is shown that strong cycle-to-cycle variations are already present in the free spray from the very beginning in all distances possibly due to the fluctuations of spray emerging from the injector nozzle. Therefore, strong cycle-to-cycle variations at the tip and on the sides of the free spray appear. The trend shows that if a step geometry constrains the spray propagation, the *Overlap Area Ratio* is higher and less cycle-to-cycle variations occur. In the 20 mm case, due to the short distance to the step geometry, the *Overlap Area Ratio* rises at around 0.4 ms (Fig. 8a) when the impinging takes place. Then, in the 30° case, the flow resistance is higher (see "Geometry Effect") leading to a high *Overlap Area Ratio*. At the time step 0.90 ms, on the right side of the 30° case (Fig. 9c), the cycle-to-cycle variations occur mainly on the boundary, whereas when the step angle is increased, the cycle-to-cycle variations affect the flow thickness (Fig. 9e,g). On the left side of the 90° case, the cycle-to-cycle variations are more severe compared to the other cases possibly due to the higher step geometry angle which causes a stronger separation between both sides depending on the spray pattern shortly before impinging (Fig. 9g). Furthermore, the

abrupt transition to the flat surface creates turbulence or the flow in out-of-plane direction possibly resulting in larger cycle-to-cycle variations which vanish soon after. In general, for all cases, the cycle-to-cycle variations on the right side increase before they decrease again (Fig. 9d,f,h).

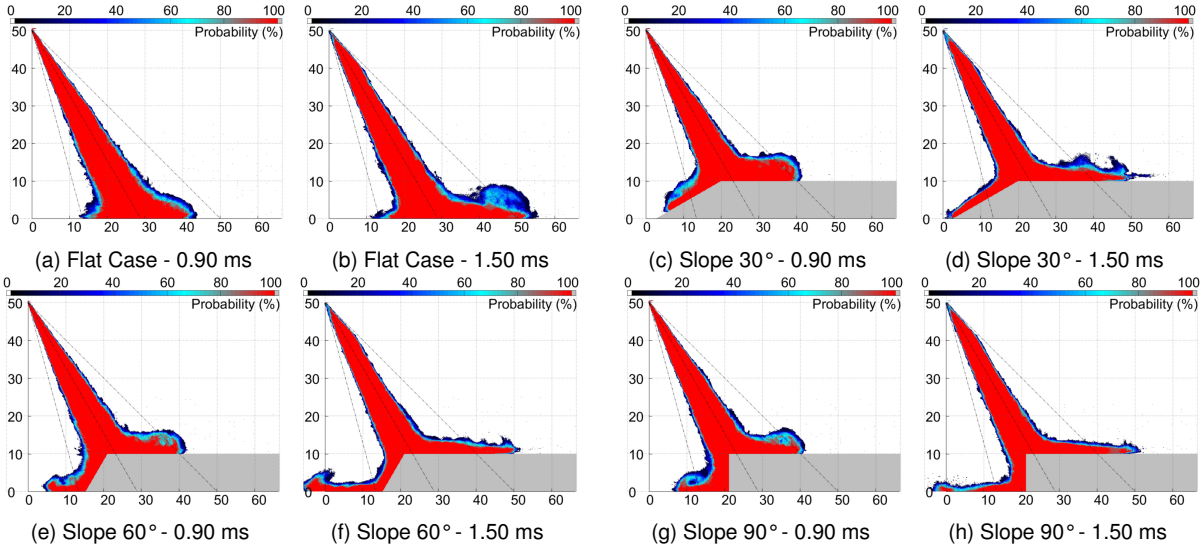

Figure 9. *Presence Probability Images* with 20 mm distance (scale of x- and y-axis in mm)

In the 35 mm case, the step geometry highly constrains the spray propagation which increases the *Overlap Area Ratio* up to 80% (Fig. 8b). The low *Overlap Area Ratio* at the 60° case is exceptional, dropping to 58% due to strong fluctuations before impinging, whereas the other cases have an *Overlap Area Ratio* of around 65%. The overall trend shows that a higher step geometry angle causes a higher *Overlap Area Ratio* and, therefore, decreases the cycle-to-cycle variations. However, a major drawback is the lack of spreading of the fuel leaving a larger area with high intensity values which leads to a deterioration of the vaporisation process. In the 40 mm case, the *Overlap Area Ratios* diverge at later stage when the spray reaches the geometry at around 0.90 ms (Fig. 8c). Figure 10b shows higher cycle-to-cycle variation compared to the 35 mm case since the propagation is less constrained. The 50 mm case shows no differences after impinging (around 0.5 ms) compared with the flat case. However, the *Probability Presence Images* show a higher probability for a higher propagation thickness or a vortex behaviour with increasing geometry angle (Fig. 10c).

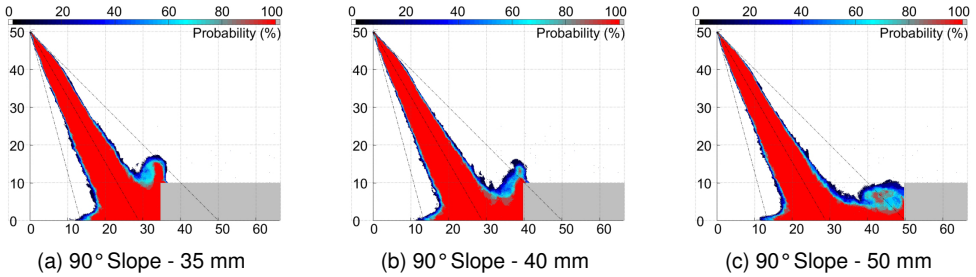

Figure 10. *Presence Probability Images* in the 90° case at time step 1.50 ms (scale of x- and y-axis in mm)

Conclusions

This research investigates experimentally the effect of surface geometry on the spray impingement and its macroscopic behaviour using high-speed mie-scattering in a constant volume chamber. The analysis of the *Multiple Cycles* included the *Wetted Length*, *Average Value Images*, and *Probability Presence Images*. The impinging process shows a "filter" effect, whereas the step geometry has an immense impact on the spray. It has the capability to stretch and constrain the spray and, therefore, plays a major role for the vaporisation process. In the 20 mm case the *Wetted Length* is enlarged up to 30% compared to the flat case which eventually supports the vaporisation process especially in the 60° slope and the 90° slope. In contrast, the 35 mm case highly constrains the spreading and reduces the propagation up to 25% compared to the flat case. Surprisingly, although the geometry constrains the propagation to the right, the left side is not influenced significantly. Consequently, the vaporisation process is strongly retarded. With longer distance between spray axis and geometry, the constraining effect fades but is still present. In order to analyse the cycle-to-cycle variations, *Probability Presence Images* are applied and *Overall Area*

Ratio are calculated. The constraining of the flow reduces the cycle-to-cycle variations and leads to higher *Overall Area Ratio*. The trend shows that increasing the geometry angle intensifies the effect and in the 35 mm case the *Overall Area Ratio* jumps up to 80% in the 90° slope. With increasing distance to the geometry, the cycle-to-cycle variations rise. Furthermore, fluctuations from the start of injection are shown which weaken with time. The results show a valuable insight of how a surface geometry affects the spray propagation. However, due to the experimental approach taken in this study, only a two-dimensional view was possible. Consequently, the next step includes a three-dimensional analysis to capture the out-of-plane movement of the spray propagation.

Acknowledgements

The authors gratefully acknowledge the financial support by the General Motors Company (USA) and the research was conducted at the National Engineering Laboratory for Automotive Electronic Technology of the Shanghai Jiao Tong University.

References

[1] Wei Du, Qiankun Zhang, Wenhua Bao, and Juejue Lou. Effects of injection pressure on spray structure after wall impingement. *Applied Thermal Engineering*, 129:1212–1218, 2018.

[2] F. Schulz and F. Beyrau. The effect of operating parameters on the formation of fuel wall films as a basis for the reduction of engine particulate emissions. *Fuel*, 238(October 2018):375–384, 2019.

[3] Zhanbo Si, Yuji Ashida, Nagisa Shimasaki, Keiya Nishida, and Youichi Ogata. Effect of cross-flow on spray structure, droplet diameter and velocity of impinging spray. *Fuel*, 234(July):592–603, 2018.

[4] Xiucheng Zhu, Le Zhao, Zhihao Zhao, Nitisha Ahuja, Jeffrey Naber, and Seong-Young Lee. An Experimental Study of Diesel Spray Impingement on a Flat Plate: Effects of Injection Conditions. In *28th European Conference on Liquid Atomization and Spray Systems (ILASS)*, pages 208–215, 2017.

[5] M.Z. Akop, Y. Zama, T. Furuhata, and M. Arai. Characteristics of adhesion of diesel fuel on impingement disk wall. Part 1: Effect of Impingement area and inclination angle of disk. *Atomization and Sprays*, 23(8):725–744, 2013.

[6] H.K. Suh, S.W. Park, and C.S. Lee. A study of the flow and atomization characteristics of impinged diesel spray on a chamber wall. *Atomization and Sprays*, 17(7):569–599, 2007.

[7] Todd D. Fansler and Scott E. Parrish. Spray measurement technology: A review. *Measurement Science and Technology*, 26(1), 2015.

[8] Le Zhao, Roberto Torelli, Xiucheng Zhu, Riccardo Scarcelli, Sibendu Som, Henry Schmidt, Jeffrey Naber, and Seong-Young Lee. An Experimental and Numerical Study of Diesel Spray Impingement on a Flat Plate. *SAE International Journal of Fuels and Lubricants*, 10(2):2017–01–0854, 2017.

[9] T Luo, H; Uchitomi, S; Nishida, K; Ogata, Y; Zhang, W and Fujikawa. Experimental Investigation on Fuel Film Formation by Spray Impingement on Flat Walls with Different Surface Roughness. *Atomization and Sprays*, 27(7):611–628, 2017.

[10] Xuesong Li, Hujie Pan, Xue Dong, David Hung, and Min Xu. Spray impingement wall film breakup by wave entrainment. *Proceedings of the Combustion Institute*, 37(3):3287–3294, 2019.

[11] Hongliang Luo, Keiya Nishida, Shintaro Uchitomi, Youichi Ogata, Wu Zhang, and Tatsuya Fujikawa. Effect of spray impingement distance on piston top fuel adhesion in direct injection gasoline engines. *International Journal of Engine Research*, pages 1–13, 2018.

[12] Hujie Pan, Di Xiao, David Hung, Min Xu, and Xuesong Li. Experimental investigations of wall jet droplet impact on spray impingement fuel fi lm formation. *Fuel*, 241(December 2018):33–41, 2019.

[13] Young Sam Shim, Gyung Min Choi, and Duck Jool Kim. Numerical and experimental study on effect of wall geometry on wall impingement process of hollow-cone fuel spray under various ambient conditions. *International Journal of Multiphase Flow*, 35(10):885–895, 2009.

[14] Qianwang Fan, Liguang Li, Zongjie Hu, and Jun Deng. Spray Characteristics and Wall-impingement Process with Different Piston Tops for the Multi-hole Injector of DISI Gasoline Engines. *SAE Technical Paper 2011-01-1222*, 2011.

[15] D. P. Towers and C. E. Towers. Cyclic variability measurements of in-cylinder engine flows using high-speed particle image velocimetry. *Measurement Science and Technology*, 15(9):1917–1925, 2004.

[16] David L.S. Hung, David M. Chmiel, and Lee E. Markle. Application of an Imaging-based Diagnostic Technique to Quantify the Fuel Spray Variations in a Direct-Injection Spark-Ignition Engine. *SAE Technical Paper No. 2003-01-0062*, 2003.

[17] Jie Zhong, David L S Hung, Zhenkan Wang, Yuyin Zhang, and Min Xu. Comparing the Cycle-to-Cycle Variations of Pulsing Spray Characteristics by Means of Ensemble Image and Probability Presence Image Analysis Techniques. In *12th Triennial International Conference on Liquid Atomization and Spray Systems*, pages 1–8, 2012.

[18] Mehmet Sezgin. Survey over image thresholding techniques and quantitative performance evaluation. *Journal of Electronic Imaging*, 13(1):146–165, 2004.

[19] Hao Chen, David L S Hung, Min Xu, and Jie Zhong. A dynamic thresholding technique for extracting the automotive spark-ignition direct-injection pulsing spray characteristics. *Journal of Visualization*, 17(3):197–209, 2014.